JACS
JOURNAL OF THE AMERICAN CHEMICAL SOCIETY

Article

pubs.acs.org/JACS

Tracking Transient Conformational States of T4 Lysozyme at Room Temperature Combining X-ray Crystallography and Site-Directed Spin Labeling

Philipp Consentius,[†] Ulrich Gohlke,[‡] Bernhard Loll,[§] Claudia Alings,[§] Robert Müller,[∥] Udo Heinemann,[‡,§] Martin Kaupp,[∥] Markus Wahl,[§] and Thomas Risse*[,†,⊥]

[†]Institute of Chemistry and Biochemistry, Freie Universität Berlin, Takustr. 3, 14195 Berlin, Germany
[‡]Max Delbrück Center for Molecular Medicine in the Helmholtz Association, Robert-Rössle-Str. 10, 13125 Berlin, Germany
[§]Institute of Chemistry and Biochemistry, Freie Universität Berlin, Takustr. 6, 14195 Berlin, Germany
[∥]Institute of Chemistry, Sekr. C7, Technische Universität Berlin, Straße des 17. Juni 135, 10623 Berlin, Germany
[⊥]Berlin Joint EPR Laboratory, Freie Universität Berlin, Takustr. 3, 14195 Berlin, Germany

Supporting Information

ABSTRACT: Proteins are dynamic molecules that can transiently adopt different conformational states. As the function of the system often depends critically on its conformational state a rigorous understanding of the correlation between structure, energetics and dynamics of the different accessible states is crucial. The biophysical characterization of such processes is, however, challenging as the excited states are often only marginally populated. We show that a combination of X-ray crystallography performed at 100 K as well as at room temperature and EPR spectroscopy on a spin-labeled single crystal allows to correlate the structures of the ground state and a thermally excited state with their thermodynamics using the variant 118R1 of T4 lysozyme as an example. In addition, it is shown that the surrounding solvent can significantly alter the energetic as well as the entropic contribution to the Gibbs free energy without major impact on the structure of both states.

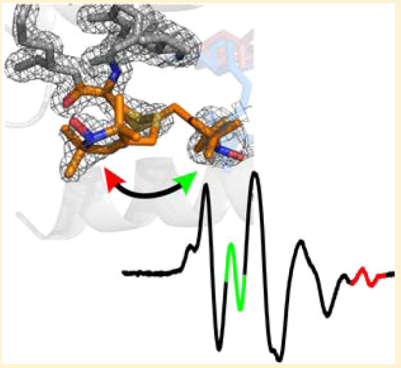

INTRODUCTION

Dynamic processes on different time and length scales characterize proteins at ambient temperature.[1−4] The dynamics of the system can be understood by a hierarchically structured, corrugated multidimensional energy hypersurface.[5] Here discussion will be limited to thermodynamically distinct macro-states ("states" from here on) separated by energy barriers of a few kT. The different states populated under physiological conditions are of great interest as they may differ in their biological function. Unraveling these correlations requires detailed knowledge of the structures as well as of the associated thermodynamics. Even though the Gibbs free energy difference of the conformational states may only be a few kT at room temperature, the associated low equilibrium population renders their biophysical characterization challenging.

X-ray crystallography is extremely powerful for reporting on structure as well as on structural changes (static as well as dynamic) in the crystalline state as long as the system is homogeneous, while disentangling inhomogeneous crystals is more complex when aiming at a quantitative description.[6,7] Relaxation-based NMR techniques have been successfully used to elucidate structural transitions between conformational states populated by a few percent only, providing evidence for both rigid-body motion of secondary structure elements as well as local unfolding.[8,9] Site-directed spin labeling (SDSL) in combination with EPR spectroscopy is another powerful spectroscopic tool to study protein structure and dynamics, which has been successfully used to characterize conformational exchange within proteins using cw- as well as pulse-spectroscopic methods.[10−12]

In addition, several methods can be employed to shift the equilibrium by perturbation of the system. It was recognized early on that the free-enthalpy landscape is modified by the experimental conditions such as temperature, pressure or solvent composition. In the case of T4 lysozyme, the population of a conformational state, being a minority species (3%) for the cavity mutant L99A (at 25 °C), is increased by additional point mutations reaching 34% and 96% population for the variants L99A/G113A and L99A/G113A/R119P, respectively.[9]

In the present study we use a combination of site directed spin labeling/EPR spectroscopy and X-ray crystallography to elucidate the structure of two conformational states, which are in thermodynamic equilibrium in the single crystal, and determine the thermodynamics of these states using T4 lysozyme single crystals. In addition, it is shown that the thermodynamics of these states can be strongly altered by the

Received: May 29, 2016
Published: September 27, 2016

DOI: 10.1021/jacs.6b05507
J. Am. Chem. Soc. 2016, 138, 12868−12875

conditions, namely the hydration level within the crystal, without noticeable impact on the structure of the corresponding states.

RESULTS AND DISCUSSION

Structure of Spin-Labeled T4 Lysozyme at Low Temperature. The low-temperature (100 K) crystal structure of the spin-labeled variant L118R1 determined at a resolution of 1.0 Å is shown in Figure 1A (PDB ID 5JDT; for side chain structure of R1 see Figure S1). The details of data collection and refinement statistics are summarized in Table S1. The structure confirms the results published by Guo et al. (PDB ID 2NTH),[13] but provides structural information at a considerably higher level of detail. The spin-labeled side chain of this variant is buried in the interior of the protein. As proposed by Guo et al.,[13] the higher volume of the spin-labeled side chain as compared to the native leucine leads to an unfolding of the short (1.5 turns) α-helix F (Figure 1A). The incorporation of the R1 side chain into the hydrophobic core of a protein was explained by the hydrophobicity of the disulfide linkage and the hydrophobic nature of the 3-pyrroline-ring structure.[4] The high-resolution structure reveals the presence of a water molecule between the oxygen atom of nitroxide and the carbonyl moiety of G107 (Figure 1B) providing clear evidence for a stabilization of the conformation by hydrogen bonding.

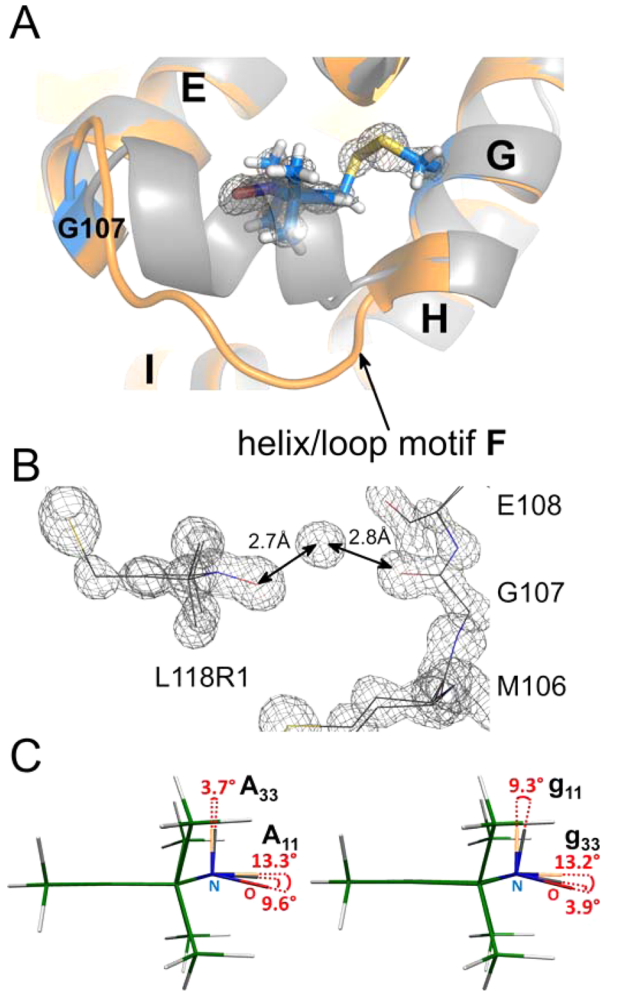

Figure 1. (A) Ribbon model based on the high-resolution crystal structure (1.0 Å; PDB ID 5JDT) of the C-terminal domain of T4 lysozyme variant L118R1 determined at 100 K (orange) superimposed by the WT* structure in gray (PDB ID 1l63). The electron density of the spin label at position 118C is shown by a $2F_o-F_c$ density difference map (σ = 1.3). (B) Structural model of the L118R1 side chain, neighboring residues M106, G107 and E108 superimposed by a $2F_o-F_c$ density difference map (σ = 1.3) in gray, which also shows electron density corresponding to a water molecule in hydrogen bonding distance. (C) Structural model of the nitroxide group from (B). The calculated directions of g- and hfi-tensor principal axes (unit vectors) are superimposed for the bended structure (gray) and a planar structure (orange). The unit vectors of the planar structure (omitted for clarity) have been centered at the nitrogen atom of the bended structure.

The electron density (Figure 1B) shows that the nitroxide ring is bent, not observed in previous crystallographic studies of spin-labeled proteins due to limited resolution (see Figure S2 for the importance of resolution to observe this effect). The latter finding is important for the analysis of spin-labeled single crystals using EPR spectroscopy as the orientation of the g- and the hyperfine interaction (hfi) matrix with respect to the crystal lattice plays a crucial role for oriented samples. In case of a planar nitroxide ring the local $C_{2\,V}$ symmetry of the NO group requires coincident interaction matrices whose x-component is oriented along the NO bond, while the z-component is oriented perpendicular to the ring. In case of a bent structure these restrictions no longer apply, which has been shown, e.g., for the TEMPO radical.[14] Hence, it is important to know the orientation of the g- and the hfi-matrix with respect to the molecule to analyze the data. This information has been obtained from quantum-chemical (DFT) calculations for both matrices using suitable model structures, as detailed in the Supporting Information. The result of these calculations is summarized in Figure 1C. With respect to a planar arrangement of the nitroxide ring, which shows the expected orientation (cf. above and SI for details), the hfi matrix in the crystal structure-based model is rotated by 3.7° around the direction of the y-component toward the bent NO bond, leading to an angle of 9.6° between the x-component and the NO-bond. Therefore, the orientation of the hfi-matrix is very close to that expected for the planar structure. The x-component of the g-matrix is similarly rotated around the y-component. It is, however, oriented much closer to the NO bond exhibiting an angle of only 3.9°. In consequence, g- and hfi-tensors are no longer collinear as expected from the reduced symmetry of the system.

Structure of Spin-Labeled T4 Lysozyme at Room Temperature. Figure 2A shows (black trace) an EPR spectrum taken at 29 °C for a specific orientation of a single crystal of the T4L variant L118R1, for which the orientation of the unit cell with respect to the static magnetic field has been determined using X-ray diffraction (for details see SI). The lack of an isotropic component in the angle-dependent EPR spectra (Figure S3) provides clear evidence for a well-defined orientation of the nitroxide residues in the crystal lattice even at room temperature. In addition, the line shape of the EPR spectrum was simulated (Figure 2A, red trace) using the structural information obtained from low-temperature crystallography. As the unit cell contains six symmetry-related molecules (space group $P3_221$), the spectra of these six molecules are superimposed. The individual line shape for a given orientation was calculated using the stochastic Liouville approach developed by Freed and co-workers.[15,16] The dynamic parameters of the simulations (Table S2), chosen to fit the spectrum of an isotropic sample of single crystals (Figure S4) best, reveal a highly restricted motion of the spin label in

DOI: 10.1021/jacs.6b05507
J. Am. Chem. Soc. 2016, 138, 12868−12875

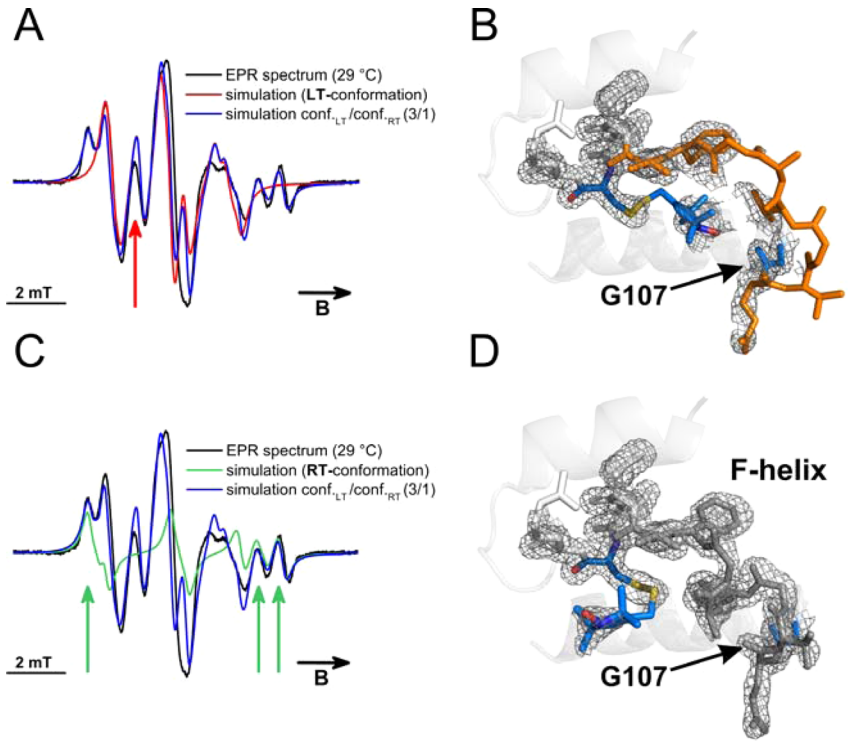

Figure 2. EPR spectrum of a T4L 118R1 single crystal (A and C, black) superimposed by line shape simulations for the LT- (red) or RT- (green) spin label conformation and a simulation using a 3:1 ratio of both (blue). The arrows indicate EPR lines corresponding exclusively the LT- (red) or the RT-conformer (green). (B and D) The two spin label conformations of side-chain L118R1 and the related local backbone changes are shown as a stick model superimposed by a $2F_o-F_c$ difference density map (σ = 1.0) in gray.

line with the expectations based on the crystal structure. The *z*-axis of the g- and hfi-matrices (collinear within the model) are aligned with the director of the order potential as readily deduced from spectral width ($\langle 2A'_{zz} \rangle$) compared to the rigid limit value (Figure S4).

With these parameters being fixed the best fit to the spectrum as shown in Figure 2A (red trace) is found for the director of the potential restricting the motion of the spin label oriented perpendicular to a "fictitious" planar nitroxide spin label, which is very close to the theoretical prediction of the direction of the z-component of the hfi-matrix. The orientation of the director with respect to the molecule is a consequence of the spin label dynamics. A detailed discussion of this aspect, however, goes beyond the scope of this article and will be presented elsewhere.[17] The simulation is able to describe some of the features of the spectrum reasonably well, while some lines, in particular at the high and low-field extremes of the spectrum, are not reflected at all. Already the line shape analysis of the spectrum in viscous solution suggested the presence of two components.[13] Therefore, the low-temperature crystal structure may not report on all the states populated at room temperature, which contribute to the EPR spectrum.

The structure of the variant L118R1 was determined at room-temperature at a resolution of 1.6 Å (PDB ID 5G27). Interestingly, two conformations of the spin label side-chain R1 are required to interpret the electron density maps shown in Figure 2B and D, respectively. The conformation of the buried spin label observed at low temperature (Figure 1A) ("LT-conformation" in the following) is also found in the electron density difference maps at room temperature (occupancy 0.3; for a comparison of the "LT-conformation" in the region of the spin label as determined by X-ray crystallography at 100 K and at RT see Figure S5). However, electron density of the spin label side chain is restricted to the disulfide region and the nitroxide ring. The loop structure clearly resolved at low temperature is no longer visible at room temperature. Despite of the lack of electron density providing clear evidence for the presence of a water molecule in between the spin label and G107 (see above), the observed electron density at the nitroxide and G107 indicates this interaction being present at room temperature, too.

The absence of defined electron density for the rest of the loop structure is expected to be due to the mobility of the loop at elevated temperature. The diffraction data (Figure 2D) revealed a second conformation (occupancy 0.7; "RT-conformation" in the following) with the spin label rotated out of the interior of the protein. Concomitantly, the loop structure transforms back into an α-helix as observed in the pseudo-wild-type (WT*) structure (PDB ID 1L63, helix F). In turn, the backbone fold of the RT-conformation corresponds to that of the WT* structure showing that, in line with reports in literature, a single point mutation can alter the conformational equilibrium of a protein significantly.[9] Electron density for the spin-labeled side chain is found up to the disulfide bridge and again for the nitroxide moiety, which allows to model the spin-labeled side chain into the electron density as shown in Figure 2D. This conformation shows no intermolecular contacts of the spin-labeled side chain to symmetry-related molecules. Its conformation is determined by a cavity on the outer surface of the protein formed by the adjacent solvent-exposed side chains K83, T115 and R119 (Figure S5). The resolved electron density of the NO moiety proves a well-defined orientation between the spin-bearing moiety and the crystal lattice, hence, the EPR spectrum of spin-labeled single crystals should be

DOI: 10.1021/jacs.6b05507
J. Am. Chem. Soc. 2016, 138, 12868−12875

angle-dependent and characterized by spatially restricted motion. Figure 2C shows the results of a simulation (green trace) using the same model assumptions concerning the dynamics of the spin label as before using the orientation of the second spin label conformation. In comparison to Figure 2A it clearly shows that the RT-conformation can account for the spectral components not described by the low-temperature conformation. In turn, the blue traces (Figure 2A, 2C) representing a superposition of both conformations with a weight of 3:1 describes the observed EPR line shape reasonably well (for a discussion about the differences between the population derived from X-ray crystallography and EPR spectroscopy see SI). It is important to note that this holds not just for the chosen angle shown here but also for the entire angle-dependent series of EPR spectra (Figure S6A). Even though the simulations can account for the line shape qualitatively, it is not possible to reach a quantitative agreement between simulation and experiment. This is not too surprising given the simple Brownian diffusion model underlying the simulations, which certainly lacks the ability to describe the details of the spin label motion on the pico- to nanosecond time encoded in the EPR line shape. The quality of the simulations shown in Figure 2 and S6A depend very sensitively on the proper choice of the orientation of the spin label as exemplarily shown in Figure S6B. Even slight misalignments by a few degrees hampers a proper description of the experimental data. Furthermore, Figure S6A shows angle dependent spectra taken for another crystal, which has a different orientation of the unit cell in the laboratory frame. The simulations use exactly the same parameters (Table S2) as well as orientation of the spin label in the unit cell as used in Figure 2 but take the different orientation of the unit cell (determined independently see methods below) into account, which renders these simulations free of adjustable parameters. Due to this behavior, the simulations presented in Figure 2 and S6A, which are based on the orientation of the spin label as determined by X-ray crystallography, clearly show that EPR spectroscopy probes the same conformational states characterized structurally by X-ray crystallography.

Thermodynamics of the Two Conformational States. From the different populations of conformational states at room temperature and 100 K observed by X-ray crystallography we conclude that both conformations are dynamically interconverted in the single crystal. In turn, the RT-conformation observed at room temperature is a thermally excited conformational state, and it is thus interesting to investigate if these conformational states are in thermodynamic equilibrium. Temperature-dependent EPR measurements (Figure 3A) show distinctly different line shapes at 29 and 5 °C, while both spectra of a temperature cycle taken at 5 °C are identical. The reversibility of the line shape during the heating cycle indicates the system to be in thermodynamic equilibrium. Mulder et al. report an exchange rate slightly above 1000 s^{-1} between two conformational states in the cavity mutant L99A of T4L (comparable equilibrium properties, see below) using NMR spectroscopic techniques.[18] Low-temperature diffraction data provide no indication for the population of the RT-conformation, and we conclude that the interconversion between the two states remains fast on the time scale of flash-cooling. From the high-resolution data it is estimated that less than 10% of the RT-conformation is present at 100 K, which indicates fast equilibration between the states down to about 260 K on the time scale of typical flash-cooling times, suggesting a low effective transition state barrier.[19]

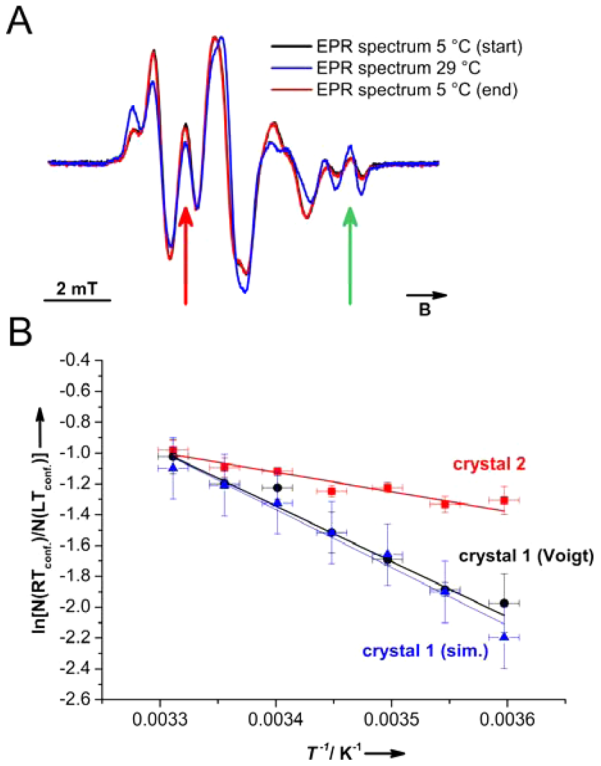

Figure 3. (A) EPR spectra of a T4L 118R1 single crystal for a temperature cycle 5, 29 and 5 °C; arrows indicate the lines for the LT- (red) and the RT- (green) component that have been used for the intensity evaluation using a set of Voigt lines (see text for details). (B) Van't Hoff plots for two T4L L118R1 single crystals of the equilibrium constant as a function of T^{-1} using temperature dependent EPR measurements to determine the relative population of the two conformers. The relative intensity of the two contributions was determined using the physical model discussed above (blue; Figure S7) and a simulation of the line shape using a series of Voigt profiles (black; Figure S8). Data for a second crystal is shown in red (for details see text).

A closer inspection of the temperature dependent line shapes reveals that the line positions, which are strongly dependent on the orientation of the spin labels as well as their local environment, are hardly changed between 5 and 29 °C, while there is a clear change of the relative intensity of lines. The latter is readily seen for the lines marked with a green and a red arrow in Figure 3A. This behavior is a direct proof for the presence of more than one orientation of the spin label within the single crystal. The analysis of the line shape discussed above (Figure 2A and C) allows to rationalize this behavior. With increasing temperature, the intensity of the spectral features associated with the RT-conformation found exclusively at the high field (green arrow, Figure 3A) increases at the expense of the LT-conformation exclusively contributing to the line marked with the red arrow in Figure 3A, as expected for a thermally excited conformational state. Two different approaches were used to quantify the relative populations of the two conformations. The first approach uses the line shape of the conformations as shown in Figure 2 and varies their relative intensity to obtain the best fit (Figure S7). The analysis gives a relative population of the RT-conformation of 25% at 29 °C and 11% at 5 °C. The simulations fail to provide a

DOI: 10.1021/jacs.6b05507
J. Am. Chem. Soc. 2016, 138, 12868−12875

quantitative description of the line shape, which leaves the question about the reliability of the relative intensity determination. The physical model clearly indicates that the lines marked with the red and green arrow in Figure 3A are exclusively due to the LT- and the RT-conformation, respectively. For an alternative evaluation, the spectra were fitted using a series of Voigt lines to account for the line shape of the spectra using a single line for the resonances marked in red and green (Figure S8). The intensity of the lines marked by the red and green arrows in Figure 3A results in populations of the RT-conformation of 26% and 12% at 29 and 5 °C, respectively, which is very similar to the population derived above. The intensity ratio of the two peaks is used as a direct measure for the equilibrium constant of a simple two-state equilibrium at different temperatures. A van't Hoff plot of the temperature dependence of the equilibrium constant deduced from this data set (Figure S8) is shown in Figure 3B for the analysis using the simulations of Figure 2 (blue symbols) and the fits using Voigt profiles (black symbols). From the slope of a linear regression to the data the enthalpy difference between the two states is 32 ± 3 kJ·mol^{-1} (blue line) and 30 ± 2 kJ·mol^{-1} (black line). The corresponding entropy difference is 95 ± 8 J·K^{-1} mol^{-1} (blue) and 91 ± 6 J·K^{-1} mol^{-1} (black), respectively. Hence, the Gibbs energy of the RT-conformation is about 3 kJ·mol^{-1} higher at 25 °C as compared to the LT-conformation. The transition between the two conformations is endothermic with significantly positive entropy. This compares well with NMR experiments analyzing the temperature dependence of exchange rates between two states of the cavity mutant L99A of T4 lysozyme. Assuming first order kinetics, the transition enthalpy and entropy were determined as 30 kJ·mol^{-1} and 72 J·K^{-1} mol^{-1}, respectively.[18] While the enthalpic contributions are identical, the entropy gain of the thermally excited conformational state is significantly smaller in case of the cavity mutant, which results in a much smaller population of the thermally excited conformational state at room temperature (3%).

Because of the positive entropy associated with the population of the thermally excited conformational states, the corresponding transitions are often described in the literature as order−disorder transitions. The structural data discussed above indicate that such a characterization is misleading in terms of the protein structure. While the RT-conformation exhibits helix F as an ordered secondary structure element, this part of the protein is disordered at room temperature in the LT-conformation. As the rest of the secondary structure elements are preserved in both conformations, the positive entropic contribution of the system in the thermally excited state cannot be associated with a more disordered state of the protein on the level of the backbone fold. It is, however, clear that within the picture of the hierarchically structured energy landscape discussed above, simple statistical thermodynamics arguments require that the number of accessible microstates within the thermally excited macro state (RT-conformation) have to be significantly higher to account for the observed positive entropy associated with this transition. At this point we can only speculate on the microscopic origin of this observation to be associated with changes in the entropic contributions of the solvent and to some extent also the side chains.

McCoy et al. have used pressure-dependent EPR measurements of the current variant of T4 lysozyme (118R1) to modulate populations of conformational substates and measure differences in compressibility.[20] The pressure-induced transition into a molten globular state of T4 lysozyme at elevated pressure was described by a simple two-state model to describe the transition from a ground state to the pressure-induced state. The current experiment implies that more than one initial state can be involved in this transition and it remains an open question to which extent the two states provide pathways into the molten globular state.

The Degree of Hydration Alters the Thermodynamic Equilibrium. An interesting observation was made for a second crystal, whose temperature-dependent line shape was measured 18 days after placing the crystal in the quartz capillary (crystals measured shortly after transfer into the glass capillary behave as discussed above). At 29 °C the system shows the same population of the conformational states described above. However, lowering the temperature results in a larger fraction of molecules in the RT-conformation. The temperature dependent line shape changes are reversible indicating that the system is in thermodynamic equilibrium. Transition enthalpy and entropy (Figure 3B red trace) are reduced to 10 kJ·mol^{-1} and 27 J·K^{-1} mol^{-1} corresponding to 33% and 29% of the values observed for freshly prepared samples, respectively. The angle-dependent EPR line shape remains unperturbed over time indicating that the reduction of both enthalpy and entropy is not associated with structural changes in the vicinity of the spin label. The latter would be picked up either by changes in the orientation of the spin label or by changes of its dynamics. The observed change is due to a slow evaporation of the water out of the capillary, which reduces the hydration level of the crystal and finally results in its disintegration observed a few days after the measurement shown here. This indicates that the burial of the spin label side chain at the expense of associated backbone disorder is less likely to happen if the crystal is less hydrated. The degree of hydration alters the thermodynamics of the two conformational substates significantly affecting both the energetics (enthalpy) and the number of accessible microstates (entropy). However, the structural properties of both states as monitored by EPR spectroscopy do not change.

■ CONCLUSION

The current study combines EPR spectroscopy and X-ray crystallography of spin-labeled protein single crystals to probe the thermodynamic equilibrium between conformational substates and it allows correlating thermodynamics and structural properties. The equilibrium is characterized by a compensation of a positive enthalpic contribution and a positive entropic part, which leads to an increased population of the conformational state with higher entropy at elevated temperature. In addition, dehydration of the system has significant impact on the thermodynamics of the two conformational states. For the current system both the enthalpy as well as entropy drop to about a third of their original values, however, without impact on the structural properties of the substates as probed by EPR spectroscopy.

■ EXPERIMENTAL SECTION

Generation of Cysteine Mutant, Gene Expression and Purification. The T4 lysozyme "pseudo-wild-type" gene carrying the C54T and C97A mutations[21] was kindly provided by the lab of Prof. Wayne L. Hubbell (UCLA). The gene was inserted into a pET-11a expression vector providing ampicillin resistance. The L118C mutation was introduced using the QuikChange method (Agilent Technologies) with a modified protocol.[22] To verify the mutation the

DOI: 10.1021/jacs.6b05507
J. Am. Chem. Soc. 2016, 138, 12868−12875

whole gene was sequenced using the Sanger method. *Escherichia coli* BL21 DE3 cells were transformed with the purified vector DNA by electroporation followed by shaking for 1 h at 37 °C. Transformants were plated on an LB-agar plate containing 100 μg/mL ampicillin and incubated at 37 °C overnight. The next day, cells were subsequently washed from the plate using preheated LB medium to inoculate 1 l of LB medium (containing 100 μg/mL ampicillin) to an OD_{600} of 0.1. For induction of gene expression isopropyl-β-D-thiogalactopyranoside (Carl Roth, Karlsruhe, Germany) was added (final concentration = 1 mM) at an OD_{600} of 1.0−1.2 and expression was allowed for 2 h at 37 °C. Cells were harvested by centrifugation at 8000*g* for 10 min, and the pellets were solubilized with lysis buffer containing 25 mM MOPS, 25 mM TRIS (pH = 7.6) and cOmplete protease inhibitor cocktail (Roche). After cell disruption (Cell Disruptor, Constant Systems) insoluble components were removed by centrifugation (40 000*g* for 30 min) and filtered (0.22 μm, Carl Roth, Karlsruhe, Germany) solution was loaded onto a HiTrap SP HP cation exchange column using an ÄKTA purifier system (GE Healthcare). Protein was eluted using a linear elution profile with elution buffer (1 M NaCl, 25 mM MOPS, 25 mM TRIS, pH 7.6). Eluted protein was further purified using a Superdex 75 prep grade gel-filtration column (GE Healthcare) equilibrated with GF buffer (25 mM MOPS, 25 mM TRIS, 100 mM NaCl, 2 mM DTT, pH = 7.6). Protein was judged to be >95% pure by a Protean TGX precast SDS-PAGE (Biorad). Protein fractions were stored at −80 °C.

Spin Labeling of T4L L118C. T4 lysozyme L118C was transferred into labeling buffer (50 mM MOPS, 25 mM NaCl, pH 6.8) using a HiTrap desalting column (GE Healthcare). Protein was incubated overnight with a 10-fold molar excess of *S*-(1-oxyl-2,2,5,5-tetramethyl-Δ^3-pyrroline-3-methyl)methanethiosulfonate (MTSSL, Santa Cruz Biotechnology). Uncoupled spin label was removed using a HiTrap desalting column equilibrated with labeling buffer. Labeled protein was concentrated to 15−20 mg/mL using an Amicon Ultra Filter Unit with a 10 kDa cutoff (Millipore).

Protein Crystallography. Single crystals were grown via the vapor diffusion method using the hanging drop setup. Reservoir solutions containing three different concentrations of K_2HPO_4 and NaH_2PO_4 mixtures (1.8 M, 2.0 and 2.2 M), 250 mM NaCl, 0.04% azide and 20 mM dithiodiethanol were set up with pH values ranging from 6.4 to 7.2. Protein solution in labeling buffer (15−20 mg/mL) was mixed with equal volumes of reservoir solution (2 μL). Two drops were placed over 1 mL reservoir solution and stored at 293 K. First crystals of 118R1 appeared in 2−4 weeks.

Best crystallization conditions comprised K_2HPO_4 and NaH_2PO_4 mixtures of 2.0 and 2.2 M with pH values of 6.8 and 7.2. For each of the four combinations 90% of the wells yielded similarly shaped, plate-like crystals between 0.1 mm (>20 crystals per drop) and 0.8 mm in the longest dimension (1−3 crystals per drop). For a good comparison of crystal size and quantity per drop at least 12 wells (one plate) of each buffer combination were set up. Crystals set up at K_2HPO_4 and NaH_2PO_4 mixtures of 2.0 and 2.2 M with a pH value of 7.2 grew predominantly to a size of approximately 0.8 mm in the longest dimension (40−60% of the wells, 1−2 crystals in each drop) and were used for single crystal experiments. Protein crystals grown at K_2HPO_4 and NaH_2PO_4 mixtures of 1.8−2.2 M with a pH value of 6.4 were in the majority of cases less than 0.5 mm in size and/or exhibited cracks and different shapes (60% or more of the wells).

For diffraction experiments at 100 K, crystals were transferred to fresh mother liquor supplemented with 10% glycerol, flash frozen, and stored in liquid nitrogen. Crystals with a size of ca. 0.5−0.7 mm in the longest direction were used for single crystal EPR measurements.

Orientation Determination of Spin-Labeled Lysozyme Crystals for EPR Spectroscopy. For characterization by EPR, single protein crystals were mounted in glass capillaries (Hilgenberg, Germany, ID 0.7 mm) and sealed with wax. The capillaries were mounted on a goniometer head, and X-ray diffraction images were collected at room temperature to determine the orientation matrix of the unit cell of the crystal. The diffraction experiments were carried out using an Xcalibur Nova O generator equipped with an Atlas CCD detector (Agilent Technologies, Yarnton, U.K.). A four circle goniometer was used to determine the kappa, omega and phi angular values that align each of the three cell axes a, b, and c of the crystal parallel with the X-ray beam. An in-house written program was used to transform the cell axes into a Cartesian coordinate system with respect to the orientation of the quartz capillary. EPR spectra taken prior and after determination of the unit cell orientation showed no change in the angle-dependent spectra. This ensured that the crystals did not change their position within the capillary during handling of the sample, and that no significant radiation damage took place.

Room Temperature Structure of L118C-R1. A complete diffraction data set was collected at 293 K using a RU-H2R X-ray generator (Rigaku, Tokyo, Japan) operated at 44 mV/58 mA and a mar345dtb image plate system (marXperts GmbH, Hamburg, Germany). Data were processed with XDS[23] followed by Aimless.[24] Initial phases were obtained by molecular replacement with Phaser[25] as part of the CCP4 suite[26] using the isomorphous structure of the T4 lysozyme L118C-R1 variant determined at 100 K (PDB ID 2NTH[27]). In order to minimize model bias, residues 107−120 of the search model were omitted, and the resulting model placed in the asymmetric unit was automatically rebuilt using ARP/wARP.[28] Iterative cycles of interactive model building with Coot[29] and refinement with BUSTER[30] led to the final model statistics summarized in Table S1. Geometrical restraints used in the refinement of the spin-labeled side chain C118 *S*-(1-oxyl-2,2,5,5-tetramethyl-Δ^3-pyrroline-3-methyl)-methanethiosulfonate linked via a disulfide bond) and the additive 2-hydroxyethyl disulfide were generated by using the grade Web Server (http://grade.globalphasing.org) that queries the Cambridge Structural Databank (CSD) with optional quantum chemical regularization. The Quality Control Check server of the Joint Center for Structural Genomics was used for the validation of the model (http://smb.slac.stanford.edu/jcsg/QC). The final model coordinates have been deposited at the Protein Data Bank with the accession number 5G27. Figures were generated with PyMOL.[31]

100 K Structure of L118C-R1. Diffraction data with a resolution of 1 Å were collected at 100 K on BL14.3 operated by the Joint Berlin MX-Laboratory at the BESSY II electron storage ring (Berlin-Adlershof, Germany).[32] X-ray data collection was performed at 100 K. Complete diffraction data were merged from separately collected high- and low-resolution data sets. For calculation of the free R-factor, a randomly generated set of 1.5% of the reflections from the diffraction data set was used and excluded from the refinement. The structure was initially refined by applying a simulated annealing protocol and in later refinement cycles by maximum-likelihood restrained refinement with PHENIX.[33,34] Model building and water picking were performed with COOT.[29] Chloride anions were identified according to peaks in an anomalous difference electron density map. Metal ions were assigned based on their coordination sphere and the distance to surrounding atoms. In final stages of the refinement, B-factors were refined anisotropically and hydrogens were generated.

EPR Spectroscopy. Electron paramagnetic resonance measurements were performed with a Bruker B-ER420 X-Band spectrometer upgraded by a Bruker ECS 041XK microwave bridge and a lock-in amplifier (Bruker ER023M). A spherical SHQ cavity (Bruker, Karlsruhe, Germany) equipped with a homemade Peltier cooling device was used for temperature-controlled measurements. For single crystal EPR a T4 lysozyme crystal was mounted in a quartz capillary (see above) located in the center of the cavity. A goniometer-like setup was designed to measure angular dependency compared to the external magnetic field. The same setup served as an attachment for the goniometer head to determine the unit cell orientation (see above). Incident microwave power of 20 mW and a modulation amplitude of 2.0 G at 100 kHz were used to acquire all spectra.

Spectral Simulations. Experimental EPR spectra were simulated using a Labview program written in house, which uses the stochastic Liouville approach developed by Freed and co-workers[35,36] as implemented in EasySpin 4.5.5[37] or a Fortran DLL created from the program package provided by the Freed laboratory. For the internal spin label motion the relation between three different coordinate frames has to be defined as described previously.[38] In short, the nitroxide tensor frame (*x*, *y*, *z*) is the frame in which g- and A-tensor

DOI: 10.1021/jacs.6b05507
J. Am. Chem. Soc. 2016, 138, 12868−12875

are diagonal (which are collinear within this implementation). The nitroxide frame is connected with the diffusion frame by three Euler angles referred to as α_D, β_D, γ_D. For anisotropic spin label motion an order potential is introduced defining one director axis defined as the z-axis of this system (z_D). Due to the symmetry of the potential the diffusion frame and the director frame are connected by a single angle θ. From the expansion coefficient of the order potential it is possible to calculate the order parameter of the potential (S).[35] For single crystals of spin labeled protein with an anisotropic motion of the spin label there is a well-defined correlation between the director of the motion and the crystal lattice. The orientation of the magnetic field, defined in the laboratory frame (the glass capillary), can be readily transformed into the frame of the crystallographic unit cell with the known orientation of the crystal. This transformation uses the three Euler angles calculated from the diffraction experiment. While the structure and the orientation of the nitroxide moiety within the unit cell is determined by X-ray diffraction, the orientation of the director of the ordering potential within the molecular as well as the nitroxide tensor frame within the diffusion frame needs to be determined. For the given system the latter can be determined from fits to the spectrum of crushed single crystals ($\alpha_D = \beta_D = \gamma_D = 0$). The isotropic spectrum is also used to determine values for the dynamic parameters used in the line-shape simulations. The orientation of the director frame with respect to the molecule remains a fitting parameter and was found to coincide with the normal of a planar nitroxide structure.

To simulate an EPR spectrum for a T4L single crystal at room temperature, the angle between the director of the ordering potential and the magnetic field (ψ) was calculated for each conformation of the spin label, which can be adopted by the six molecules in the unit cell. Using the dynamic and magnetic parameters (see Table S2) and the angle ψ spectra were calculated for each molecule and summed up to give a composite spectrum for a given orientation of the spin label. The values for the order parameter S and the rotational diffusion rates log R_{xx}, log R_{yy} and log R_{zz} were determined by fitting the spectrum of an isotropic suspension of microcrystals. These values were validated by a global optimization to a set of four spectra taken at different angles.

Quantum-Chemical Calculations. All electronic-structure calculations have been performed using density functional theory (DFT) methods. Structure optimizations were done at the B3LYP-D3(BJ)/def2-TZVPP[39−43] level of theory, employing the empirical dispersion corrections of Grimme (DFT-D3) with Becke−Johnson damping (BJ).[44,45] Subsequent single-point calculations used the B3LYP functional in conjunction with IGLO-III[46] basis sets for all atoms. Optimizations and single-point calculations were done with the TURBOMOLE program, version 6.3.1.[47−50] For the calculation of hfi-(A-) and g-tensor components (Figure S10, S11 and S12) the B3LYP/IGLO-III unrestricted Kohn−Sham orbitals were transferred to the in-house MAG-ReSpect program, version 2.1,[51] by suitable interface routines. A common gauge at the nitrogen atom was used for the g-tensor calculations. In all calculations a simplified structural model of the nitroxide-containing L118R1 side chain has been employed, in which the sulfur link (see Figures S1 and S9) was replaced by a hydrogen atom.

■ ASSOCIATED CONTENT

Supporting Information

The Supporting Information is available free of charge on the ACS Publications website at DOI: 10.1021/jacs.6b05507.

Results of additional EPR and X-ray diffraction experiments; structural models to support the interpretation of the results (PDF)

■ AUTHOR INFORMATION

Corresponding Author

*risse@chemie.fu-berlin.de

Notes

The authors declare no competing financial interest.

■ ACKNOWLEDGMENTS

M.K, R.M, and T.R. acknowledge support by the cluster of excellence (314) Unifying Concepts in Catalysis (UniCat) funded by the DFG and hosted at the Technische Universität Berlin. The molecular biology part of this study was done in the molecular biophysics laboratory of the Department of Physics of FU Berlin. We acknowledge access to beamline BL14.3 of the BESSY II storage ring (Berlin, Germany) via the Joint Berlin MX-Laboratory sponsored by the Helmholtz Zentrum Berlin für Materialien und Energie, the Freie Universität Berlin, the Humboldt-Universität zu Berlin, the Max-Delbrück Centrum, and the Leibniz-Institut für Molekulare Pharmakologie.

■ REFERENCES

(1) Henzler-Wildman, K.; Kern, D. *Nature* **2007**, *450*, 964.
(2) Baldwin, A. J.; Kay, L. E. *Nat. Chem. Biol.* **2009**, *5*, 808.
(3) Cafiso, D. S. *Acc. Chem. Res.* **2014**, *47*, 3102.
(4) López, C. J.; Yang, Z.; Altenbach, C.; Hubbell, W. L. *Proc. Natl. Acad. Sci. U. S. A.* **2013**, *110*, E4306.
(5) Frauenfelder, H.; Sligar, S. G.; Wolynes, P. G. *Science* **1991**, *254*, 1598.
(6) Merski, M.; Fischer, M.; Balius, T. E.; Eidam, O.; Shoichet, B. K. *Proc. Natl. Acad. Sci. U. S. A.* **2015**, *112*, 5039.
(7) Bourgeois, D.; Royant, A. *Curr. Opin. Struct. Biol.* **2005**, *15*, 538.
(8) Neudecker, P.; Robustelli, P.; Cavalli, A.; Walsh, P.; Lundström, P.; Zarrine-Afsar, A.; Sharpe, S.; Vendruscolo, M.; Kay, L. E. *Science* **2012**, *336*, 362.
(9) Bouvignies, G.; Vallurupalli, P.; Hansen, D. F.; Correia, B. E.; Lange, O.; Bah, A.; Vernon, R. M.; Dahlquist, F. W.; Baker, D.; Kay, L. E. *Nature* **2011**, *477*, 111.
(10) Jeschke, G. *Annu. Rev. Phys. Chem.* **2012**, *63*, 419.
(11) Hubbell, W. L.; López, C. J.; Altenbach, C.; Yang, Z. *Curr. Opin. Struct. Biol.* **2013**, *23*, 725.
(12) Mchaourab, H. S.; Steed, P. R.; Kazmier, K. *Structure* **2011**, *19*, 1549.
(13) Guo, Z. F.; Cascio, D.; Hideg, K.; Kalai, T.; Hubbell, W. L. *Protein Sci.* **2007**, *16*, 1069.
(14) Bordeaux, D.; Lajzerowicz-Bonneteau, J.; Briere, R.; Lemaire, H.; Rassat, A. *Org. Magn. Reson.* **1973**, *5*, 47.
(15) Budil, D. E.; Lee, S.; Saxena, S.; Freed, J. H. *J. Magn. Reson., Ser. A* **1996**, *120*, 155.
(16) Schneider, D. J.; Freed, J. H. In *Lasers Molecules Methods*; John Wiley & Sons: New York, 1989; Vol. *73*, p 387.
(17) Consentius, P.; Loll, B.; Gohlke, U.; Müller, R.; Kaupp, M.; Müller, C.; Risse, T., unpublished.
(18) Mulder, F. A. A.; Mittermaier, A.; Hon, B.; Dahlquist, F. W.; Kay, L. E. *Nat. Struct. Biol.* **2001**, *8*, 932.
(19) Kim, C. U.; Tate, M. W.; Gruner, S. M. *Proc. Natl. Acad. Sci. U. S. A.* **2011**, *108*, 20897.
(20) McCoy, J.; Hubbell, W. L. *Proc. Natl. Acad. Sci. U. S. A.* **2011**, *108*, 1331.
(21) Matsumura, M.; Matthews, B. W. *Science* **1989**, *243*, 792.
(22) Ho, S. N.; Hunt, H. D.; Horton, R. M.; Pullen, J. K.; Pease, L. R. *Gene* **1989**, *77*, 51.
(23) Kabsch, W. In *International Tables for Crystallography*; Rossmann, M., Arnold, E., Eds.; Wiley Interscience, 2006; Vol. F, 25.2.9, p 730.
(24) Evans, P. R.; Murshudov, G. N. *Acta Crystallogr., Sect. D: Biol. Crystallogr.* **2013**, *69*, 1204.
(25) McCoy, A. J.; Grosse-Kunstleve, R. W.; Adams, P. D.; Winn, M. D.; Storoni, L. C.; Read, R. J. *J. Appl. Crystallogr.* **2007**, *40*, 658.
(26) Winn, M. D.; Ballard, C. C.; Cowtan, K. D.; Dodson, E. J.; Emsley, P.; Evans, P. R.; Keegan, R. M.; Krissinel, E. B.; Leslie, A. G.;

DOI: 10.1021/jacs.6b05507
J. Am. Chem. Soc. 2016, 138, 12868−12875

McCoy, A.; McNicholas, S. J.; Murshudov, G. N.; Pannu, N. S.; Potterton, E. A.; Powell, H. R.; Read, R. J.; Vagin, A.; Wilson, K. S. *Acta Crystallogr., Sect. D: Biol. Crystallogr.* **2011**, *67*, 235.
(27) Guo, Z.; Cascio, D.; Hideg, K.; Kalai, T.; Hubbell, W. L. *Protein Sci.* **2007**, *16*, 1069.
(28) Langer, G.; Cohen, S. X.; Lamzin, V. S.; Perrakis, A. *Nat. Protoc.* **2008**, *3*, 1171.
(29) Emsley, P.; Cowtan, K. *Acta Crystallogr., Sect. D: Biol. Crystallogr.* **2004**, *60*, 2126.
(30) Bricogne, G.; Brandl, M.; Flensburg, C.; Keller, P.; Paciorek, W.; Roversi, P.; Sharff, A.; Smart, O.; Vonrhein, C.; Womack, T. O. *BUSTER*, Vers. 2.10.1., 2014.
(31) *The PyMOL Molecular Graphics System*, Vers. 1.8; Schrödinger LLC.
(32) Mueller, U.; Forster, R.; Hellmig, M.; Huschmann, F. U.; Kastner, A.; Malecki, P.; Puhringer, S.; Rower, M.; Sparta, K.; Steffien, M.; Uhlein, M.; Wilk, P.; Weiss, M. S. *Eur. Phys. J. Plus* **2015**, *130*, 141.
(33) Adams, P. D.; Afonine, P. V.; Bunkoczi, G.; Chen, V. B.; Davis, I. W.; Echols, N.; Headd, J. J.; Hung, L. W.; Kapral, G. J.; Grosse-Kunstleve, R. W.; McCoy, A. J.; Moriarty, N. W.; Oeffner, R.; Read, R. J.; Richardson, D. C.; Richardson, J. S.; Terwilliger, T. C.; Zwart, P. H. *Acta Crystallogr., Sect. D: Biol. Crystallogr.* **2010**, *66*, 213.
(34) Afonine, P. V.; Grosse-Kunstleve, R. W.; Echols, N.; Headd, J. J.; Moriarty, N. W.; Mustyakimov, M.; Terwilliger, T. C.; Urzhumtsev, A.; Zwart, P. H.; Adams, P. D. *Acta Crystallogr., Sect. D: Biol. Crystallogr.* **2012**, *68*, 352.
(35) Schneider, D. J.; Freed, J. H. In *Spin Labeling Theory and Applications*; Berliner, L. J., Reuben, J., Eds.; Wiley: New York, NY, 1989; p 1.
(36) Budil, D. E.; Lee, S.; Saxena, S.; Freed, J. H. *J. Magn. Reson., Ser. A* **1996**, *120*, 155.
(37) Stoll, S.; Schweiger, A. *J. Magn. Reson.* **2006**, *178*, 42.
(38) Columbus, L.; Kalai, T.; Jeko, J.; Hideg, K.; Hubbell, W. L. *Biochemistry* **2001**, *40*, 3828.
(39) Becke, A. D. *Phys. Rev. A: At., Mol., Opt. Phys.* **1988**, *38*, 3098.
(40) Lee, C.; Yang, W.; Parr, R. G. *Phys. Rev. B: Condens. Matter Mater. Phys.* **1988**, *37*, 785.
(41) Becke, A. D. *J. Chem. Phys.* **1993**, *98*, 5648.
(42) Schäfer, A.; Huber, C.; Ahlrichs, R. *J. Chem. Phys.* **1994**, *100*, 5829.
(43) Weigend, F.; Häser, M.; Patzelt, H.; Ahlrichs, R. *Chem. Phys. Lett.* **1998**, *294*, 143.
(44) Grimme, S.; Antony, J.; Ehrlich, S.; Krieg, H. *J. Chem. Phys.* **2010**, *132*, 154104.
(45) Grimme, S.; Ehrlich, S.; Goerigk, L. *J. Comput. Chem.* **2011**, *32*, 1456.
(46) Kutzelnigg, W.; Fleischer, U.; Schindler, M. In *NMR Basic Principles and Progress*; Diehl, P., Fluck, E., Günther, H., Kosfeld, R., Eds.; Springer-Verlag: Heidelberg, 1990; Vol. *23*, p 165.
(47) Ahlrichs, R.; Bär, M.; Häser, M.; Horn, H.; Kölmel, C. *Chem. Phys. Lett.* **1989**, *162*, 165.
(48) Deglmann, P.; May, K.; Furche, F.; Ahlrichs, R. *Chem. Phys. Lett.* **2004**, *384*, 103.
(49) Treutler, O.; Ahlrichs, R. *J. Chem. Phys.* **1995**, *102*, 346.
(50) Von Arnim, M.; Ahlrichs, R. *J. Comput. Chem.* **1998**, *19*, 1746.
(51) Malkin, V. G.; Malkina, O. L.; Reviakine, R.; Arbouznikov, A. V.; Kaupp, M.; Schimmelpfennig, B.; Malkin, I.; Repisky, M.; Komorovsky, S.; Hrobárik, P.; Malkin, E.; Helgaker, T.; Ruud, K. *MAG-ReSpect*, Vers. 2.1, 2005.

DOI: 10.1021/jacs.6b05507
J. Am. Chem. Soc. 2016, 138, 12868−12875